Atmos. Meas. Tech. Discuss., https://doi.org/10.5194/amt-2019-57
Manuscript under review for journal Atmos. Meas. Tech.
Discussion started: 7 March 2019

Atmospheric Measurement Techniques Discussions

Year-round stratospheric aerosol backscatter ratios calculated from lidar measurements above Northern Norway

Arvid Brand[1], Gerd Baumgarten[1], Jens Fiedler[1], Franz-Josef Lübken[1], Christian von Savigny[2], and Jacob Zalach[2]

[1]Leibniz Institut für Atmoshärenphysik an der Universität Rostock, Schlossstraße 6, 18223 Kühlungsborn
[2]Universität Greifswald, Felix-Hausdorff-Str. 6, 17489 Greifswald

Correspondence to: Arvid Brand (brand@iap-kborn.de)

Abstract.

In this work, the processing of a year-round stratospheric sulphate aerosol (SSA) dataset from day- and nighttime lidar measurements is presented. The SSA layer is of fundamental importance for the radiative balance of the atmosphere. The layer is found at altitudes between the tropopause and about 30 km. We use a state of the art Doppler Rayleigh-Mie-Raman lidar at the ALOMAR research station located in Northern Norway (69° N, 16° E) to observe the aerosol layer and derive microphysical properties. The lidar allows the investigation of SSA from small spatial and temporal scales to decadal variations. The aerosol backscatter ratio is derived by using a multi-wavelength approach and different scattering processes. Here we introduce a method for the extension of the dataset throughout the summer where measurements have to be performed under permanent daytime conditions. We calculate backscatter ratios from color ratios of elastic scattered light at the wavelengths 355, 532 and 1064 nm. These color ratios are corrected using an average backscatter ratio profile at 355 nm from the years 2000 to 2018. Thereby, we are able to extend the dataset from 2883 hours of nighttime data to 7273 hours of total data time between 2000 and 2018.

1 Introduction

The role of SSA for the radiative balance and the ozone chemistry of the atmosphere is widely accepted. Long-term observations of the stratospheric aerosol layer are crucial for the analysis of global atmospheric temperature and ozone layer variability (Thomason and Peter, 2006; Solomon et al., 2011). First in situ measurements of SSA have been performed by Christian Junge and coworkers (Junge and Manson, 1961). They found a distinct layer between 15 and 25 km altitude with a peak at 20 km (Junge et al., 1961a, b). The stratospheric aerosol layer is therefore often referred to as "Junge-layer". Remote sensing of the aerosol layer by lidar was started by Bartusek and Gambling (1971). Global satellite observations of SSA began in the late 1970s (reviewed by Thomason and Peter (2006) and Kremser et al. (2016)).

Atmos. Meas. Tech. Discuss., https://doi.org/10.5194/amt-2019-57
Manuscript under review for journal Atmos. Meas. Tech.
Discussion started: 7 March 2019

Atmospheric Measurement Techniques Discussions

The upper boundary is determined by the evaporation of the aerosol particles due to rising temperatures in the stratosphere as well as sedimentation (Hofmann et al., 1985). The tropopause is generally known as the base of the aerosol layer since the upper tropospheric aerosol levels are often much lower than in the stratosphere (Kremser et al., 2016).

Understanding SSA formation and life-cycle in the stratosphere are impossible without understanding the processes controlling sulfur in the stratosphere. Stratospheric sulfur can be found in a broad variety of gaseous molecules, such as carbon disulfide (CS_2), sulfur dioxide (SO_2), carbonyl sulfide (OCS) and sulfuric acid (H_2SO_4) (English et al., 2011). The composition of SSA is dominated by about 75 $\%$ sulfuric acid/water ($H_2SO_4-H_2O$) solution droplets (Thomason and Peter, 2006). In volcanically quiescient periods, the main source for these droplets are CS_2 and OCS. These compounds are emitted at the surface and lifted into the stratosphere by deep convection and the Brewer-Dobson circulation (Khaykin et al., 2017). They then react in multiple steps via SO_2 into sulfuric acid (Kremser et al., 2016). Stratospheric aerosols are primarily washed out by sedimentation and through the quasi-isentropic transport of air masses in tropopause folds (Thomason and Peter, 2006).

Moreover, the stratospheric sulphate aerosol variability is dominated by major volcanic eruptions injecting sulfur directly into the stratosphere. These episodic but powerful eruptions can overlay the permanent stratospheric aerosol layer (referred to as "background" aerosol) for years and can have a global cooling effect on the surface in the order of a few tenths of a degree Celsius (Robock and Mao, 1995). That aerosols from large volcanic eruptions can have global effects was first determined by worldwide observations of optical phenomena following the eruption of Krakatau in 1883 (Judd et al., 1888). After the Mount Pinatubo eruption in 1991 the stratospheric sulfur burden was increased by a factor of 60 above background levels and remained heightened by a factor of 10 well into 1993 (McCormick et al., 1995).

The long-term development of SSA has been discussed in various studies (reviewed by Kremser et al. (2016)). Observations covering the timespan between 1970 and 2004 did not show significant changes in the background aerosol (Deshler et al., 2006). Newer works show rising levels of SSA since 2002 (Hofmann et al., 2009; Vernier et al., 2011; Trickl et al., 2013; von Savigny et al., 2015). The reason for this increase is being debated. Originally the rise of the aerosol levels was connected to a fast increase in Asian sulfur emissions, lifted into the stratosphere though deep convection in the Asian monsoon (Hofmann et al., 2009). Also, more recent studies show an increase in nonvolcanic aerosol compounds inside of the Asian Tropopause Aerosol Layer (ATAL). This layer occurs during the northern summer above the Asian monsoon (Vernier et al., 2015; Yu et al., 2015). Vernier et al. (2011) showed with the help of global satellite observations, that weaker eruptions also inflect the stratospheric aerosol layer. Several studies have shown, that although these moderate eruptions are much less powerful than El Chichón or Pinatubo and the effect on stratospheric aerosol levels are much smaller, they have an impact on global surface temperatures (Solomon et al., 2011; Fyfe et al., 2013; Santer et al., 2014, 2015; Andersson et al., 2015). Accurate long-term measurements are essential to quantify background, volcanic and anthropogenic changes in the stratospheric aerosol layer.

While balloon- or rocket-borne instruments deliver information only sporadically and satellites have to average data over a large area, lidar measurements are capable of ensuring the continuity and coherence of the stratospheric aerosol record at a certain location.

The structure of the paper is as follows, in section 2 the lidar, as well as the data processing steps, are described. Following, in section 3 the calculation of the aerosol backscatter ratio R and the color ratio CR is explained. We then move on to section

Atmos. Meas. Tech. Discuss., https://doi.org/10.5194/amt-2019-57
Manuscript under review for journal Atmos. Meas. Tech.
Discussion started: 7 March 2019

Atmospheric Measurement Techniques Discussions

4, where the methodology of the extension of the dataset throughout the summer is discussed, followed by the results in section 5 and conclusions.

2 ALOMAR RMR lidar

The Rayleigh-Mie-Raman lidar is one of the core instruments at the Arctic Lidar Observatory for Middle Atmosphere Research (ALOMAR) on the island of Andøya in Northern Norway (69.3° N, 16.0° E). The main task is to perform studies of the Arctic middle atmosphere over altitudes of about 15 to 90 km (von Zahn et al., 2000). The instrument is optimized to measure simultaneously atmospheric temperatures, winds and aerosols (Fiedler et al., 2008; Baumgarten, 2010). The RMR lidar consists of two independent power lasers and two receiving telescopes and is therefore also referred to as a twin-lidar system. The emitting wavelengths of the two Nd:YAG power lasers are 1064, 532 and 355 nm. They produce 30 pulses per second with a duration of about 10 ns. The telescopes are independently tiltable from zenith pointing up to 30° off-zenith. One telescope can be tilted to the north-west quadrant (NWT[1]) and the other one to the south-east quadrant (SET[2]), to perform measurements in a common volume with sounding rockets (Baumgarten et al., 2002). To maximize the overlap of the field of view of the telescopes with the laser beams, the beams are emitted into the atmosphere coaxially with the line of sight of the telescopes.

The light collected by the telescopes is alternatingly coupled into the detection system by a segmented mirror rotating with 30 Hz. Fig 1 shows a schematic overview of the detection system. The light is separated into different wavelengths using dichroic mirrors. The detection system is capable of detecting seven wavelengths during night-time (elastic: 355, 532, 1064 nm; inelastic: 387, 529, 530, 608 nm) and three elastic wavelengths during daytime (355, 532, 1064 nm) using etalon systems to oppress the solar background (for details see von Zahn et al. (2000)). The three elastic wavelengths have been used before for calculating properties of ice particles at the mesopause (e.g. von Cossart et al. (1999); Baumgarten et al. (2008)). For the study of aerosols in the stratosphere, the channels were extended with intensity cascaded detectors to allow for simultaneous measurements from the troposphere to the mesosphere. Then, the generated signals are processed by a complex data acquisition and control system. We calculate the measurement uncertainty from the actual count of photons assuming a Poisson distribution. This uncertainty of the raw counts is then propagated through the following processing steps:

- Deadtime correction - After a photon is counted by a detector, a minimum time span has to go by before another photon can be counted. This deadtime τ is about 20 to 50 ns for the used detectors. The corrected number of counted photons N is calculated from the deadtime and the count rate N_{count}:

$$N = \frac{1}{1 - \tau \cdot N_{count}} \tag{1}$$

- Background subtraction - The telescopes also collect light from scattered solar photons, stars or airglow. Therefore the signal from far above 100 km, where no laser light is been received, is subtracted from the signal in all altitudes.

[1] north west telescope
[2] south east telescope

Atmos. Meas. Tech. Discuss., https://doi.org/10.5194/amt-2019-57
Manuscript under review for journal Atmos. Meas. Tech.
Discussion started: 7 March 2019

Atmospheric Measurement Techniques Discussions

Table 1. Overview of the ALOMAR RMR lidar counters used for this work. Indices represent the particular wavelength.

combined counter	counter on optical bench	scattering process	daylight capability
U_{355}	UL_{355}	elastic (Rayleigh and Mie)	yes
	UM_{355}		
	UH_{355}		
V_{532}	VL_{532}	elastic (Rayleigh and Mie)	yes
	VM_{532}		
	VH_{532}		
I_{1064}	IL_{1064}	elastic (Rayleigh and Mie)	yes
	IH_{1064}		
UVR_{387}	UVR_{387}	inelastic (Raman)	no
VVR_{608}	$VVRL_{608}$	inelastic (Raman)	no
	$VVRH_{608}$		

- Correction for Rayleigh-Extinction - The laser light is continuously scattered out of the beam. This also happens for the scattered, downward propagating light. The magnitude of this effect depends on the wavelength and the density of the atmosphere (Penndorf, 1957).

- Correction for Ozone-Extinction - Amongst other wavelengths, stratospheric Ozone absorbs light between 400 and 900 nm (Brion et al., 1998). The wavelengths affected most strongly (by the Chappuis bands) are 532 and 608 nm. The O_3 absorption cross sections are taken from Gorshelev et al. (2014).

The correction for both, Rayleigh- and ozone-extinction, is done using European Centre for Medium-Range Weather Forecasts (ECMWF) density and ozone mixing ratio data. We use data from the Integrated Forecasting System available per hour for the location of ALOMAR. Afterwards, the data is converted to a 5 min and 150 m grid for each detector. The signals generated by a detector, processed and corrected are in the following referred to as a counter.

3 Methodology

In order to retrieve vertical profiles of stratospheric aerosol, we first combine the counters with different sensitivity for each wavelength. This is done by normalizing the various energy cascaded levels and averaging the counters in altitude ranges, in which more than one counter is available. A relative measurement uncertainty of 0.1 is defining the uppermost altitude for each counter. The process is shown in Fig. 2. As a result, we get one continuous profile for each wavelength. A tabular overview of the different counters can be seen in table 1.

Atmos. Meas. Tech. Discuss., https://doi.org/10.5194/amt-2019-57
Manuscript under review for journal Atmos. Meas. Tech.
Discussion started: 7 March 2019

Atmospheric Measurement Techniques Discussions

The retrieval is based on the Fernald-Klett inversion method (Fernald, 1984; Klett, 1985). The backscatter ratio R is derived as the ratio of the sum of aerosol and molecular backscattering to molecular backscattering:

$$R = \frac{\beta_{aero} + \beta_{mol}}{\beta_{mol}} = 1 + \frac{\beta_{aero}}{\beta_{mol}}, \tag{2}$$

where β_{aero} and β_{mol} are the aerosol and molecular backscatter coefficients, respectively. Inelastic scattering only occurs on molecules (Raman, 1928), therefore we are able to use an inelastic counter signal for the denominator of equation 2. Elastic scattering on the other hand appears on both, aerosols and molecules (Rayleigh, 1871, 1899). Hence it is possible to use a elastic counter signal as the numerator of equation 2.

Due to the much lower scattering cross section for inelastic scattering, the signal for inelastic counters can be some orders of magnitude smaller. Thus the signals have to be normalised in an aerosol-free altitude range on order to eliminate an aerosol influence on the normalization. This altitude is considered to be above 30 km (McCormick et al., 1984; Barnes and Hofmann, 1997; Khaykin et al., 2017). We choose a normalization altitude from 34 to 38 km because the inelastic signal is still strong enough and the total aerosol layer is found below. The normalization is performed in a two-step iteration. First, we calculate the mean signal ratio in the normalization range, then we limit the signal ratio data in the normalization range to those altitudes within 1-sigma of the mean signal ratio. This procedure reduces the effect of an aerosol reaching up to the normalization layer. More details on this are discussed in section 5. Accordingly, equation 2 yields:

$$R = \left[\frac{Signal\ (inelastic)}{Signal\ (elastic)}\right]_{z(R=1)} \cdot \frac{Signal\ (elastic)}{Signal\ (inelastic)}, \tag{3}$$

where $z(R=1)$ is the normalization altitude between 34 and 38 km.

Furthermore the calculation of a color ratio CR is of importance. It describes a ratio of two elastic signals and is computed as follows:

$$CR = \left[\frac{Signal\ (elastic)(\lambda_0)}{Signal\ (elastic)(\lambda_1)}\right]_{z(R=1)} \cdot \frac{Signal\ (elastic)(\lambda_1)}{Signal\ (elastic)(\lambda_0)}, \tag{4}$$

with λ_o and λ_1 being two elastic scattered lidar wavelengths.

There are multiple combinations of possible elastic and inelastic signals. In this work, we focus on 1064 nm as the elastic signal due to the highest aerosol backscatter signal at this wavelength and 387 nm as the inelastic signal because it is only weak affected by ozone extinction ($R_{1064/387}$).

Since only stratospheric aerosols are investigated in this study, the data is reduced to altitudes above the tropopause. This is done by using the ECMWF data for the dynamical and the thermal tropopause for each time step. The backscatter ratio data is reduced to altitudes higher than the larger of these two tropopause values to exclude tropospheric air.

Using this method also detects polar stratospheric clouds (PSC) (see Peter (1997) for details). In winter, these clouds occur over ALOMAR frequently. The calculated backscatter ratio R of the PSCs is one order of magnitude higher than for SSA and therefore overlying the background aerosol. Thus, measurements with clear evidence of PSCs are removed from the dataset.

An example of a R measurement over 80 hours in February 2018 is shown in Fig. 3. The result draws a highly dynamic picture of the stratospheric aerosol layer. There are several layers thinner than one km of aerosol above 20 km visible over days.

Atmos. Meas. Tech. Discuss., https://doi.org/10.5194/amt-2019-57
Manuscript under review for journal Atmos. Meas. Tech.
Discussion started: 7 March 2019

Atmospheric Measurement Techniques Discussions

It should be emphasized that these layers are not connected with PSCs since the temperatures at the time were above 210 K and therefore too high for PSC formation. The measurement only shows stratospheric background aerosol. With the described methodology an investigation of stratospheric aerosol above ALOMAR on unprecedented time scales becomes possible.

4 Dataset expansion to daylight conditions

The ALOMAR RMR lidar is situated at 69.3° N, i.e. north of the Polar circle, requiring day configuration all summer. The stratospheric aerosol retrieval uses an inelastic scattering counter which is available at night only (see table 1). In order to retrieve a solid year-round dataset, we use a multi-color approach and correct a year-round available color ratio CR of two elastic scattering counters.

The starting point are the profiles depicted in Fig. 4. Shown are two backscatter ratios (green: $R_{1064/387}$, blue: $R_{355/387}$), which are calculated by using equation 3. This equation is also applicable if the inelastic signal is not available during the whole measurement run, i.e. if the daytime configuration was used partly during the run. Also shown is a color ratio (red: $CR_{1064/355}$) which is calculated by using equation 4. The blue $R_{355/387}$ profile shows an aerosol part in the 355 nm Signal which explains the difference between red ($CR_{1064/355}$) and blue ($R_{1064/387}$) profile. As mentioned before, the red $R_{1064/355}$ profile is available year-round due to the daylight capability of the elastic channels of the ALOMAR RMR lidar.

Figure 5 shows 103 suitable $R_{355/387}$ averaged profiles from measurements runs between 2000 and 2018, which cover a total of 1789 h of measurement. In order to find these profiles the dataset has been filtered for measurement runs without PSCs and with a relative backscatter ratio measurement uncertainty smaller than one percent. The $R_{355/387}$ profiles show a linear behaviour towards $R \to 1$ at $z = 34$ km. Therefore a mean profile ($\tilde{R}_{355}(z)$) is calculated and fitted linearly with the altitude z:

$$\tilde{R}_{355}(z) = \frac{z - 407.95\ \mathrm{km}}{-374.16\ \mathrm{km}} \tag{5}$$

The fit $\tilde{R}_{355}(z)$ is used to correct the $CR_{1064/355}$ profiles with the following equation:

$$R_{1064/355} = CR_{1064/355} \cdot \tilde{R}_{355}(z) \tag{6}$$

with $R_{1064/355}$ being the approximated backscatter ratio at 1064 nm. The result for the measurement is shown in Fig. 6. The new purple drawn profile $R_{1064/355}$ matches the true backscatter ratio (green: $R_{1064/387}$) well within measurement uncertainty. The higher total uncertainty of the corrected profile is caused by the measurement uncertainty of the color ratio profile, the measurement uncertainties of the $\tilde{R}_{355}(z)$ linear fit and of the correction which is calculated as the mean difference between $R_{1064/387}$ and $R_{1064/355}$ for each altitude. This difference is shown in Fig. 7 for each of the 103 measurement runs where both these profiles are available between 2000 and 2018. The resulting standard deviation of this distribution is drawn as a red shade and defines the uncertainty for a single $R_{1064/355}$ profile as shown in the purple shaded area in Fig. 6.

The same correction can be done for the 532 nm branch of the lidar system. This is also shown in Fig. 4 and Fig 6. In this case, an approximated backscatter ratio $R_{532/355}$ (orange) is calculated from the corresponding color ratio $CR_{532/355}$ (yellow)

Atmos. Meas. Tech. Discuss., https://doi.org/10.5194/amt-2019-57
Manuscript under review for journal Atmos. Meas. Tech.
Discussion started: 7 March 2019

Atmospheric Measurement Techniques Discussions

and the correction fit $\tilde{R}_{355}(z)$ to extend the $R_{355/387}$ backscatter ratio data (cyan) year-round. It is derived by the equation:

$$R_{532/355} = CR_{532/355} \cdot \tilde{R}_{355}(z) \tag{7}$$

In conclusion, a new dataset (R_{1064}) is composed, consisting of $R_{1064/387}$ profiles when available and $R_{1064/355}$ profiles when not. The result is a solid year-round dataset of stratospheric aerosol backscatter profiles.

5 Results

To show the performance of the new procedure of compiling a dataset of aerosol backscatter ratios R_{1064} we investigate the data from the years 2014 to 2017. By choosing four recent years of lidar operations, we can well cover a typical seasonal cycle of stratospheric aerosol. A total of 232 measurement runs were performed, collecting data we can use for the analysis. In 24 of those runs PSCs were detected and thus these runs were excluded. The 208 remaining runs represent 3646 hours of measurement. Of these measurements, 2391 hours were performed during daytime while 1255 hours were performed during nighttime. Fig. 8 shows the available monthly data time for the R_{1064} and $R_{1064/387}$ dataset between 2014 and 2017. For nearly every month a gain in data time is reached by extending the $R_{1064/387}$ dataset to the R_{1064} dataset. The lone exception is the month of December, where only 3 hours of data are available for both datasets. We define a lower limit of data availability of 10 hours per month in order to obtain representative data. Furthermore, the standard error of the monthly mean backscatter ratio ($\sigma_{\overline{R}}$) may not exceed 0.02. This value is not reached for any monthly average of the R_{1064} dataset, where $\sigma_{\overline{R}}$ is below 0.01 for every month. For the monthly average of the $R_{1064/387}$ dataset for April of 2014 to 2017 $\sigma_{\overline{R}}$ is about 0.025 due to a small dataset of only 35 hours with high variability. For all other months, the standard error is also below 0.01. These criteria lead to a lack of data in the $R_{1064/387}$ dataset for the months of April to July, and for December for both datasets.

An example of the effect of the extension of the stratospheric aerosol dataset is shown in Fig. 9 and Fig. 10. Both these figures show a seasonal cycle of aerosol backscatter ratio over the time span 2014 to 2017. The first picture for the ratio $R_{1064/387}$ clearly lacks data between April and July, where no nighttime measurements were performed. The data illustrated in Fig. 9 was calculated from 79 measurement runs between 2014 and 2017.

Fig.10 depicts the aerosol backscatter ratio for R_{1064}. This new dataset, obtained by applying the procedure described in section 4, covers the whole annual cycle in stratospheric aerosol above ALOMAR. The R_{1064} dataset is based on the aforementioned 79 measurement runs with $R_{1064/387}$ plus 129 measurement runs with $R_{1064/355}$ measured in daylight conditions between 2014 and 2017, adding up to a total of 208 measurement runs.

For 2014 to 2017, the R_{1064} and the $R_{1064/387}$ datasets show strong occasional aerosol loads in September in the stratosphere between 12 km and 18 km. These high aerosol levels originate in Canadian wildfires and therefore strong pyrocumulonimbus activity over western Canada. The smoke reached Europe 10 days after its injection in the lower stratosphere (see Ansmann et al. (2018) for further details) and was detected by the lidar. During the winter months, November to March the aerosol layer is located at significantly lower altitudes. In this time the layer is found mostly in between 12 km to 22 km. Stratospheric air is sinking within the polar vortex in winter. If the ALOMAR observatory is located under the polar vortex, this effect is seen in the aerosol data. Both datasets cover this behaviour well.

Atmos. Meas. Tech. Discuss., https://doi.org/10.5194/amt-2019-57
Manuscript under review for journal Atmos. Meas. Tech.
Discussion started: 7 March 2019

Atmospheric Measurement Techniques Discussions

We have detected that the stratospheric aerosol reaches well above 30 km especially during summer. We find backscatter ratio values in R_{1064} above 30 km of about 1.05 with a typical uncertainty of 0.02. A presence of aerosol in these altitude ranges is clearly given and should be taken into account in future studies for determining the normalization altitude when calculating R.

6 Conclusions

The ALOMAR RMR lidar is suited to perform stratospheric aerosol measurements throughout the day and the year in the northern polar region. With the lidar, we continuously determine aerosol backscatter ratios (R_{1064}) between the tropopause and 34 km. The accuracy of these backscatter profiles is dominated by the random error of the backscatter signal. We calculate the highest uncertainties for very short lidar measurement runs (measurement time under one hour). In these rare cases the uncertainty for the stratospheric aerosol backscatter ratio varies from 0.1 at 10 km to 0.8 at 34 km. Most lidar measurements are longer. For a 5 h measurement the uncertainty does not exceed 0.02 over the complete altitude range.

The challenge of calculating backscatter profiles above ALOMAR during summer was solved by correcting a color ratio available during daylight measurements with a long time mean $\tilde{R}_{355}(z)$ profile fit. The uncertainties of the resulting profiles are dominated by the uncertainty of the correction and result to 0.06 at 11 km and 0.02 at 34 km for a monthly average of R_{1064}. The difference between $R_{1064/355}$ and $R_{1064/387}$ gets smaller with the altitude approaching the normalization range of 34 km, hence, so does the uncertainty of the R_{1064} backscatter profile. As the R_{1064} dataset is built by the available $R_{1064/387}$ data plus corrected $R_{1064/355}$ data it differs little from $R_{1064/387}$ between September and March. Significant differences occur between April and August due to the addition of large data time (see Fig. 8). The used correction of the aerosol backscatter data will lead to an underestimation of the aerosol in cases of strong aerosol loads. This is due to the fact, that the correction fit profile $\tilde{R}_{355}(z)$ was derived from background profiles with common aerosol loads (see Fig. 5). Depending on altitude, the correction has a total effect on the backscatter ratio from 6 % at 10 km to no effect at 34 km.

Using the described methodology, it is possible to investigate the stratospheric aerosol layer above ALOMAR in various ways. For example a single lidar measurement shows strong variations in aerosol backscatter ratio on a 5 minute time resolution (See Fig. 3). Another example is the first year-round cycle of the stratospheric aerosol measured by lidar in the Arctic. The new dataset also allows the investigation up to decadal scales. Exemplarily, a comparison of monthly mean backscatter ratio from 2014 to 2017 for the nighttime dataset $R_{1064/387}$ (Fig. 9) and the new year-round dataset R_{1064} (Fig. 10) was carried out. The extension of the dataset fills the aerosol backscatter ratio data gap during summer and leads to a year-round dataset.

Between 2000 and 2018 lidar measurements at ALOMAR where performed on a regular bases. In this timespan we gain 2883 hours of usable data time for the $R_{1064/387}$ dataset. For the same time this data time raises to 7273 hours for the R_{1064} dataset.

In future work, also aerosol backscatter coefficients and extinction coefficients will be derived from the dataset.

Code and data availability. The datasets used in this study can be obtained by contacting the first author

Competing interests. The authors declare that they have no conflict of interest.

Acknowledgements. This work benefited from the excellent support of J. Hildebrand, M. Gerding and the dedicated staff at the ALOMAR observatory. The European Centre for Medium-Range Weather Forecasts (ECMWF) is gratefully acknowledged for providing the data. This project is supported by DFG (Deutsche Forschungsgesellschaft, Projektnummer 312991878)

Atmos. Meas. Tech. Discuss., https://doi.org/10.5194/amt-2019-57
Manuscript under review for journal Atmos. Meas. Tech.
Discussion started: 7 March 2019

References

Andersson, S. M., Martinsson, B. G., Vernier, J.-P., Friberg, J., Brenninkmeijer, C. A., Hermann, M., Van Velthoven, P. F., and Zahn, A.: Significant radiative impact of volcanic aerosol in the lowermost stratosphere, Nature communications, 6, 7692, 2015.

Ansmann, A., Baars, H., Chudnovsky, A., Mattis, I., Veselovskii, I., Haarig, M., Seifert, P., Engelmann, R., and Wandinger, U.: Extreme levels of Canadian wildfire smoke in the stratosphere over central Europe on 21–22 August 2017, Atmospheric Chemistry and Physics, 18, 11 831–11 845, 2018.

Barnes, J. E. and Hofmann, D. J.: Lidar measurements of stratospheric aerosol over Mauna Loa Observatory, Geophysical Research Letters, 24, 1923–1926, 1997.

Bartusek, K. and Gambling, D.: Simultaneous measurements of stratospheric aerosols using lidar and the twilight technique, Journal of Atmospheric and Terrestrial Physics, 33, 1415–1430, doi:10.1016/0021-9169(71)90013-4, http://www.sciencedirect.com/science/article/pii/0021916971900134, 1971.

Baumgarten, G.: Doppler Rayleigh/Mie/Raman lidar for wind and temperature measurements in the middle atmosphere up to 80 km, Atmospheric Measurement Techniques, 3, 1509–1518, 2010.

Baumgarten, G., Lübken, F.-J., and Fricke, K.: First observation of one noctilucent cloud by a twin lidar in two different directions, Ann. Geophys., 20, 1863–1868, 2002.

Baumgarten, G., Fiedler, J., Lübken, F.-J., and von Cossart, G.: Particle properties and water content of noctilucent clouds and their interannual variation, J. Geophys. Res., 113, D06203, doi:10.1029/2007JD008884, 2008.

Brion, J., Chakir, A., Charbonnier, J., Daumont, D., Parisse, C., and Malicet, J.: Absorption spectra measurements for the ozone molecule in the 350–830 nm region, Journal of atmospheric chemistry, 30, 291–299, 1998.

Deshler, T., Anderson-Sprecher, R., Jäger, H., Barnes, J., Hofmann, D. J., Clemesha, B., Simonich, D., Osborn, M., Grainger, R., and Godin-Beekmann, S.: Trends in the nonvolcanic component of stratospheric aerosol over the period 1971–2004, Journal of Geophysical Research: Atmospheres, 111, 2006.

English, J., Toon, O., Mills, M., and Yu, F.: Microphysical simulations of new particle formation in the upper troposphere and lower stratosphere, Atmos. Chem. Phys, 11, 9303–9322, 2011.

Fernald, F. G.: Analysis of atmospheric lidar observations: some comments, Appl. Opt., 23, 652–653, 1984.

Fiedler, J., Baumgarten, G., and von Cossart, G.: A middle atmosphere lidar for multi-parameter measurements at a remote site, 24th ILRC, pp. 824–827, 2008.

Fyfe, J., Salzen, K. v., Cole, J., Gillett, N., and Vernier, J.-P.: Surface response to stratospheric aerosol changes in a coupled atmosphere–ocean model, Geophysical Research Letters, 40, 584–588, 2013.

Gorshelev, V., Serdyuchenko, A., Weber, M., Chehade, W., and Burrows, J.: High spectral resolution ozone absorption cross-sections–Part 1: Measurements, data analysis and comparison with previous measurements around 293 K, Atmospheric Measurement Techniques, 7, 609–624, 2014.

Hofmann, D., Rosen, J., and Gringel, W.: Delayed production of sulfuric acid condensation nuclei in the polar stratosphere from El Chichon volcanic vapors, Journal of Geophysical Research: Atmospheres, 90, 2341–2354, 1985.

Hofmann, D., Barnes, J., O'Neill, M., Trudeau, M., and Neely, R.: Increase in background stratospheric aerosol observed with lidar at Mauna Loa Observatory and Boulder, Colorado, Geophysical Research Letters, 36, 2009.

Judd, J. W., Strachey, R., Wharton, W. J. L., Evans, F. J., Russell, F. A. R., Archibald, D., and Whipple, G. M.: The Eruption of Krakatoa: And Subsequent Phenomena, Trübner & Company, 1888.

Junge, C. E. and Manson, J. E.: Stratospheric aerosol studies, Journal of Geophysical Research, 66, 2163–2182, 1961.

Junge, C. E., Chagnon, C. W., and Manson, J. E.: Stratospheric aerosols, Journal of Meteorology, 18, 81–108, 1961a.

Junge, C. E., Chagnon, C. W., and Manson, J. E.: A World-wide Stratospheric Aerosol Layer, Science, 133, 1478–1479, doi:10.1126/science.133.3463.1478-a, http://science.sciencemag.org/content/133/3463/1478.2, 1961b.

Khaykin, S. M., Godin-Beekmann, S., Keckhut, P., Hauchecorne, A., Jumelet, J., Vernier, J.-P., Bourassa, A., Degenstein, D. A., Rieger, L. A., Bingen, C., et al.: Variability and evolution of the midlatitude stratospheric aerosol budget from 22 years of ground-based lidar and satellite observations, Atmospheric Chemistry and Physics, 17, 1829–1845, 2017.

Klett, J. D.: Lidar inversion with variable backscatter/extinction ratios, Appl. Opt., 24, 1638–1643, doi:10.1364/AO.24.001638, http://ao.osa.org/abstract.cfm?URI=ao-24-11-1638, 1985.

Kremser, S., Thomason, L. W., Hobe, M., Hermann, M., Deshler, T., Timmreck, C., Toohey, M., Stenke, A., Schwarz, J. P., Weigel, R., Fueglistaler, S., Prata, F. J., Vernier, J., Schlager, H., Barnes, J. E., Fairlie, D., Palm, M., Mahieu, E., Notholt, J., Rex, M., Bingen, C., Vanhellemont, F., Bourassa, A., Plane, J. M. C., Klocke, D., Carn, S. A., Clarisse, L., Trickl, T., Neely, R., James, A. D., Rieger, L., Wilson, J. C., Meland, B., and Antuna-Marrero, J.-C.: Stratospheric aerosol—Observations, processes, and impact on climate, Reviews of Geophysics, 54, 278–335, doi:10.1002/2015RG000511, https://agupubs.onlinelibrary.wiley.com/doi/abs/10.1002/2015RG000511, 2016.

McCormick, M., Swissler, T., Fuller, W., Hunt, W., and Osborn, M.: Airborne and ground-based lidar measurements of the El Chichon stratospheric aerosol from 90 N to 56 S, Geofisica Internacional, 23, 1984.

McCormick, M. P., Thomason, L. W., and Trepte, C. R.: Atmospheric effects of the Mt Pinatubo eruption, Nature, 373, 399, 1995.

Penndorf, R.: Tables of the refractive index for standard air and the Rayleigh scattering coefficient for the spectral region between 0.2 and 20.0 μ and their application to atmospheric optics, Josa, 47, 176–182, 1957.

Peter, T.: Microphysics and heterogeneous chemistry of polar stratospheric clouds, Annual Review of Physical Chemistry, 48, 785–822, 1997.

Raman, C. V.: A new radiation, 1928.

Rayleigh, L.: On the scattering of light by small particles, The London, Edinburgh, and Dublin Philosophical Magazine and Journal of Science, 41, 447–454, 1871.

Rayleigh, L.: XXXIV. On the transmission of light through an atmosphere containing small particles in suspension, and on the origin of the blue of the sky, The London, Edinburgh, and Dublin Philosophical Magazine and Journal of Science, 47, 375–384, 1899.

Robock, A. and Mao, J.: The volcanic signal in surface temperature observations, Journal of Climate, 8, 1086–1103, 1995.

Santer, B. D., Bonfils, C., Painter, J. F., Zelinka, M. D., Mears, C., Solomon, S., Schmidt, G. A., Fyfe, J. C., Cole, J. N., Nazarenko, L., et al.: Volcanic contribution to decadal changes in tropospheric temperature, Nature Geoscience, 7, 185, 2014.

Santer, B. D., Solomon, S., Bonfils, C., Zelinka, M. D., Painter, J. F., Beltran, F., Fyfe, J. C., Johannesson, G., Mears, C., Ridley, D. A., et al.: Observed multivariable signals of late 20th and early 21st century volcanic activity, Geophysical Research Letters, 42, 500–509, 2015.

Solomon, S., Daniel, J. S., Neely, R. R., Vernier, J.-P., Dutton, E. G., and Thomason, L. W.: The Persistently Variable "Background" Stratospheric Aerosol Layer and Global Climate Change, Science, 333, 866–870, doi:10.1126/science.1206027, http://science.sciencemag.org/content/333/6044/866, 2011.

Thomason, L. and Peter, T.: Assessment of stratospheric aerosol properties (ASAP), Available online: www. sparc-climate.org/publications/sparc-reports/(accessed on 1 December 2015), 2006.

Trickl, T., Giehl, H., Jäger, H., and Vogelmann, H.: 35 yr of stratospheric aerosol measurements at Garmisch-Partenkirchen: from Fuego to Eyjafjallajökull, and beyond, Atmospheric Chemistry and Physics, 13, 5205–5225, 2013.

Vernier, J.-P., Thomason, L. W., Pommereau, J.-P., Bourassa, A., Pelon, J., Garnier, A., Hauchecorne, A., Blanot, L., Trepte, C., Degenstein, D., et al.: Major influence of tropical volcanic eruptions on the stratospheric aerosol layer during the last decade, Geophysical Research Letters, 38, 2011.

Vernier, J.-P., Fairlie, T., Natarajan, M., Wienhold, F., Bian, J., Martinsson, B., Crumeyrolle, S., Thomason, L., and Bedka, K.: Increase in upper tropospheric and lower stratospheric aerosol levels and its potential connection with Asian pollution, Journal of Geophysical Research: Atmospheres, 120, 1608–1619, 2015.

von Cossart, G., Fiedler, J., and von Zahn, U.: Size distribution of NLC particles as determined from 3–color observations of NLC by ground-based Lidar, Geophys. Res. Lett., 26(11), 1513–1516, doi:10.1029/1999GL900226, 1999.

von Savigny, C., Ernst, F., Rozanov, A., Hommel, R., Eichmann, K.-U., Rozanov, V., Burrows, J., and Thomason, L.: Improved stratospheric aerosol extinction profiles from SCIAMACHY: validation and sample results, Atmospheric Measurement Techniques, 8, 5223–5235, 2015.

von Zahn, U., von Cossart, G., Fiedler, J., Fricke, K. H., Nelke, G., Baumgarten, G., Rees, D., Hauchecorne, A., and Adolfsen, K.: The ALOMAR Rayleigh/Mie/Raman lidar: objectives, configuration, and performance, Annales Geophysicae, 18, 815–833, doi:10.1007/s00585-000-0815-2, https://doi.org/10.1007/s00585-000-0815-2, 2000.

Yu, P., Toon, O. B., Neely, R. R., Martinsson, B. G., and Brenninkmeijer, C. A.: Composition and physical properties of the Asian tropopause aerosol layer and the North American tropospheric aerosol layer, Geophysical research letters, 42, 2540–2546, 2015.

Atmos. Meas. Tech. Discuss., https://doi.org/10.5194/amt-2019-57
Manuscript under review for journal Atmos. Meas. Tech.
Discussion started: 7 March 2019

Atmospheric Measurement Techniques Discussions

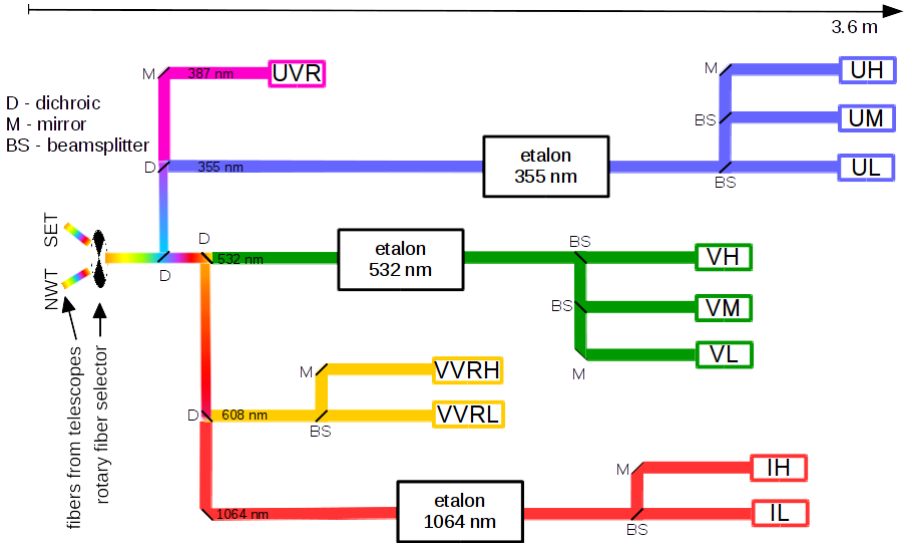

Figure 1. Simplified overview of the polychromatic detection system of the ALOMAR RMR lidar. The light collected by the telescopes enters the optical bench on the middle left side of the sketch. It is then separated by wavelength via dichroic mirrors (D) and intensity via beam splitters (BS). In daylight conditions, the light is guided through etalons to suppress solar background. At the end of each branch, the photons are converted to electrical pulses using avalanche photo diodes and photomultiplier tubes and then counted by the detection electronics. The identification mark for these detectors is built as follows: first letter: spectral range (U-ultraviolet, V-visible, I-infrared), last letter: sensitivity (L-low, M-middle, H-high). Further letters "VR" for vibrational Raman,

Atmos. Meas. Tech. Discuss., https://doi.org/10.5194/amt-2019-57
Manuscript under review for journal Atmos. Meas. Tech.
Discussion started: 7 March 2019

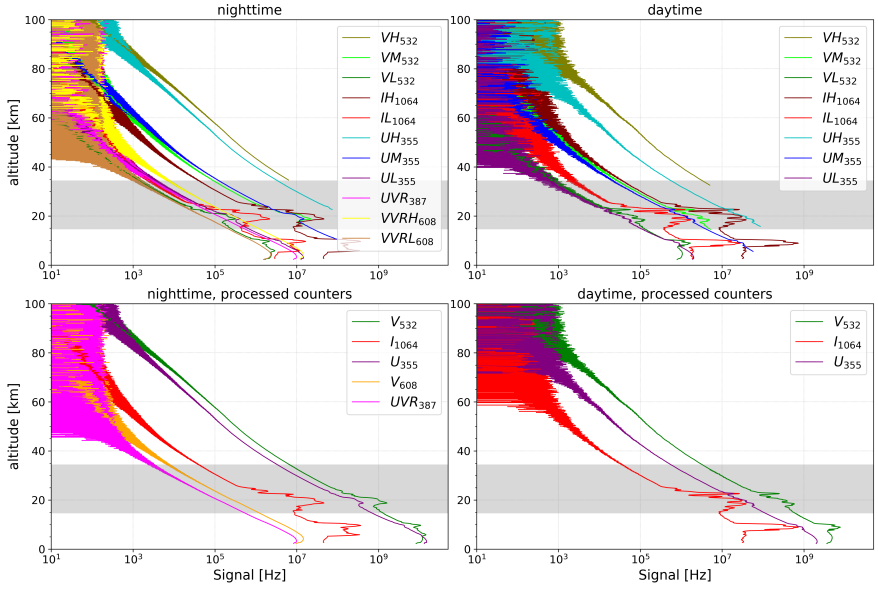

Figure 2. Averaged altitude profiles of backscattered signals for different counters of the RMR lidar for a 17 hours long measurement in January 2018. The upper panels show the original count rate, the lower ones the resulting profiles after combining the signals of the different altitude ranges. On the left side for nighttime data and on the right side for daytime data. The altitude range of the stratospheric aerosol layer is shown in gray. The increase in the profiles below 30 km is caused by tropospheric and polar stratospheric clouds. The plots show an average of both laser/telescope systems of the lidar.

Atmos. Meas. Tech. Discuss., https://doi.org/10.5194/amt-2019-57
Manuscript under review for journal Atmos. Meas. Tech.
Discussion started: 7 March 2019

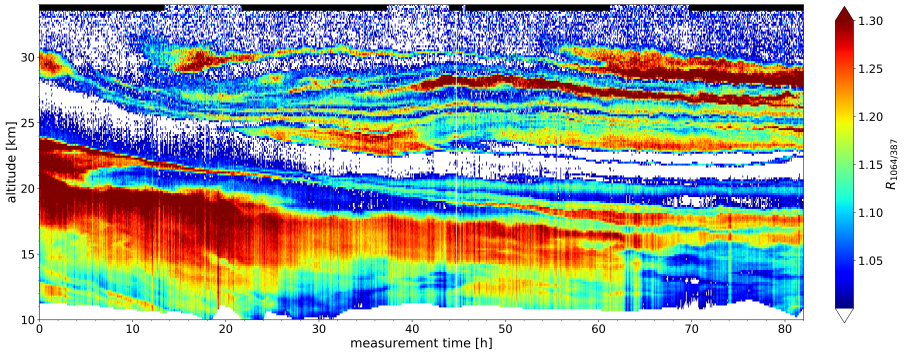

Figure 3. Stratospheric aerosol backscatter ratio ($R_{1064/387}$) for a measurement starting 17:30 UT on February 18th 2018. The time resolution is 5 minutes and the altitude resolution is 150 m. Black bars at the top indicate nighttime configuration. At the bottom end, data is cut at the tropopause.

Atmos. Meas. Tech. Discuss., https://doi.org/10.5194/amt-2019-57
Manuscript under review for journal Atmos. Meas. Tech.
Discussion started: 7 March 2019

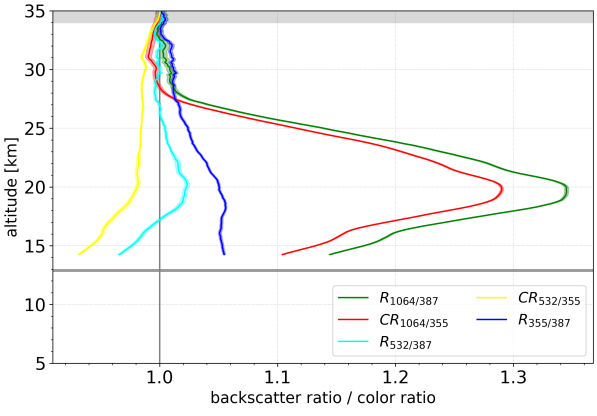

Figure 4. Backscatter ratio and color ratio profiles for a 97 hour measurement starting 07:45 UT on October 10th 2015. 46 hours of the data have been measured in daytime configuration and 51 hour in nighttime configuration. The green ($R_{1064/387}$) and the cyan ($R_{532/387}$) curves show the backscatter ratio which is not available in summer. The red ($CR_{1064/355}$) and the yellow ($CR_{532/355}$) curves show a color ratio, where aerosol signal is present in both counters. The blue curve shows a $R_{355/387}$ backscatter ratio which is used to correct the $CR_{1064/355}$ and $CR_{532/355}$ color ratios. The grey area at the top indicates part of the normalization altitude. Coloured shaded areas around the lines indicate the measurement uncertainty. The grey line at 13 km indicates the tropopause.

Atmos. Meas. Tech. Discuss., https://doi.org/10.5194/amt-2019-57
Manuscript under review for journal Atmos. Meas. Tech.
Discussion started: 7 March 2019

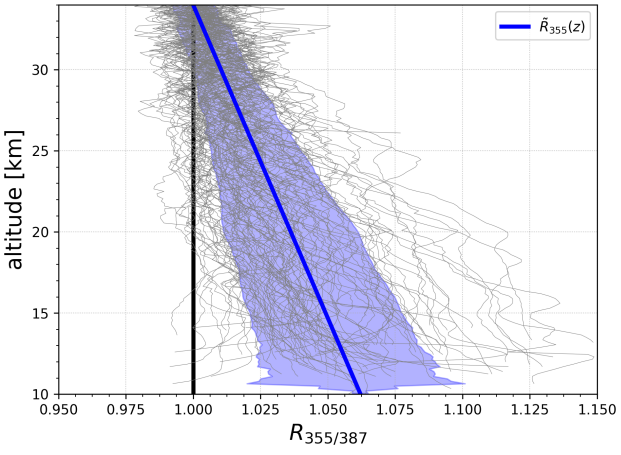

Figure 5. $R_{355/387}$ profiles from 2000 to 2018 (grey). Each line is a nighttime measurement run average. The total nighttime measurement time of all profiles is 1789 hours. Profiles are filtered for runs without PSC. The linear fit of the mean profile is drawn in blue ($\tilde{R}_{355}(z)$) with the uncertainty being the standard deviation of the $R_{355/387}$ profiles.

Atmos. Meas. Tech. Discuss., https://doi.org/10.5194/amt-2019-57
Manuscript under review for journal Atmos. Meas. Tech.
Discussion started: 7 March 2019

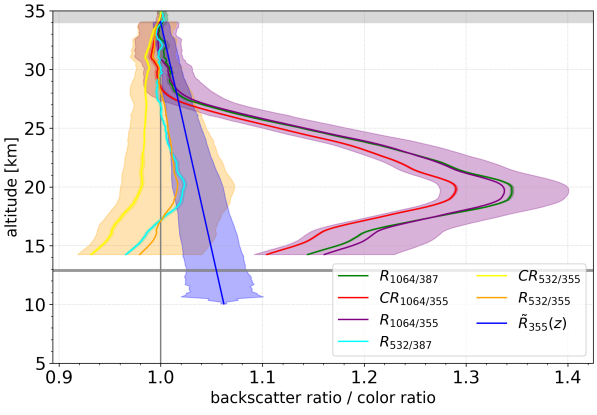

Figure 6. Backscatter ratio and color ratio profiles for a 97 hour measurement starting 07:45 UT on October 10th 2015. 46 hours of the data have been measured in daytime configuration and 51 hour in nighttime configuration. The green ($R_{1064/387}$) and the cyan ($R_{532/387}$) curves show the backscatter ratio which is not available in summer. The red ($CR_{1064/355}$) and the yellow ($CR_{532/355}$) curves show a color ratio, where aerosol signal is present in both counters. The blue curve shows the $\tilde{R}_{355}(z)$ average backscatter ratio which is used to correct the $CR_{1064/355}$ and $CR_{532/355}$ color ratios, using equation 6. The grey area at the top indicates part of the normalization altitude. Coloured shaded areas around the lines indicate the measurement uncertainty. The grey line at 13 km indicates the tropopause. This results in the corrected color ratios $R_{1064/355}$ (purple) and $R_{532/355}$ (orange) for this measurement.

Atmos. Meas. Tech. Discuss., https://doi.org/10.5194/amt-2019-57
Manuscript under review for journal Atmos. Meas. Tech.
Discussion started: 7 March 2019

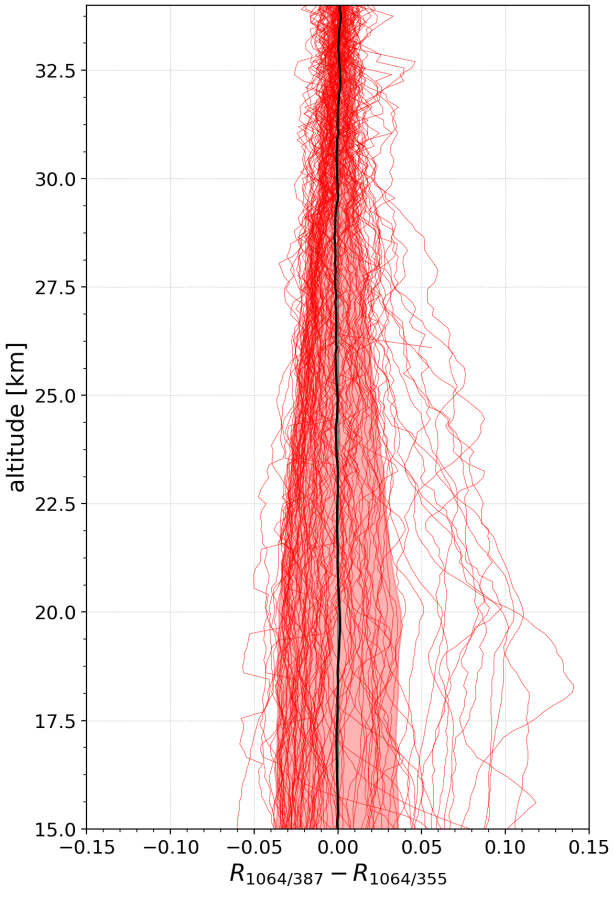

Figure 7. Altitude profiles of the difference of $R_{1064/387}$ and $R_{1064/355}$ for each measurement between 2000 and 2018 where both ratios are available (red lines, 103 profiles). The red shadowed area shows the standard deviation of the profiles. The black line depicts the mean difference.

Atmos. Meas. Tech. Discuss., https://doi.org/10.5194/amt-2019-57
Manuscript under review for journal Atmos. Meas. Tech.
Discussion started: 7 March 2019

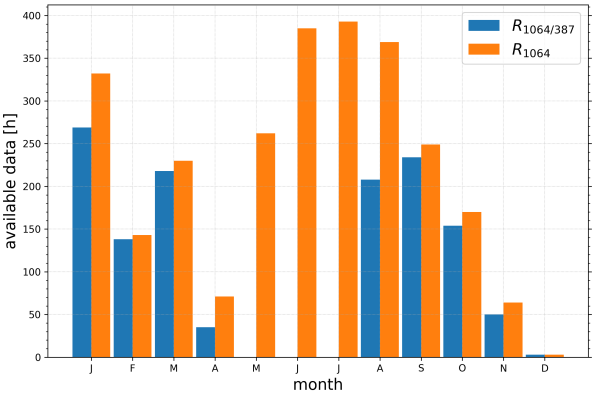

Figure 8. Time of available data for each month in the years 2014 to 2017 for $R_{1064/387}$ (blue) and R_{1064} (orange).

Atmos. Meas. Tech. Discuss., https://doi.org/10.5194/amt-2019-57
Manuscript under review for journal Atmos. Meas. Tech.
Discussion started: 7 March 2019

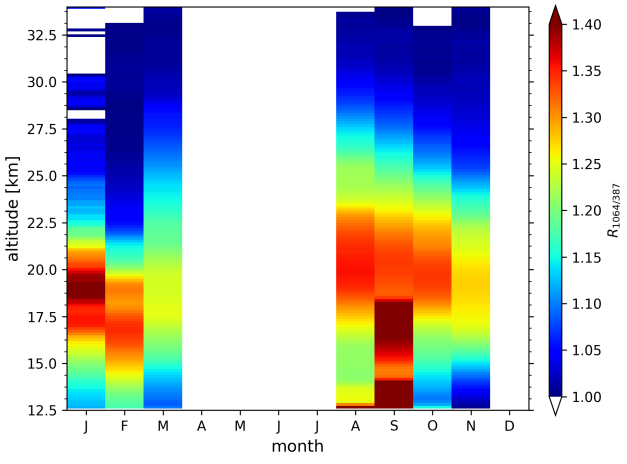

Figure 9. Mean seasonal cycle of aerosol backscatter ratio $R_{1064/387}$ over the time span 2014 to 2017. The backscatter ratio was calculated from hourly averaged lidar data and averaged per month afterwards. The seasonal cycle is calculated from 79 measurement runs with a total of 1255 hours.

Atmos. Meas. Tech. Discuss., https://doi.org/10.5194/amt-2019-57
Manuscript under review for journal Atmos. Meas. Tech.
Discussion started: 7 March 2019

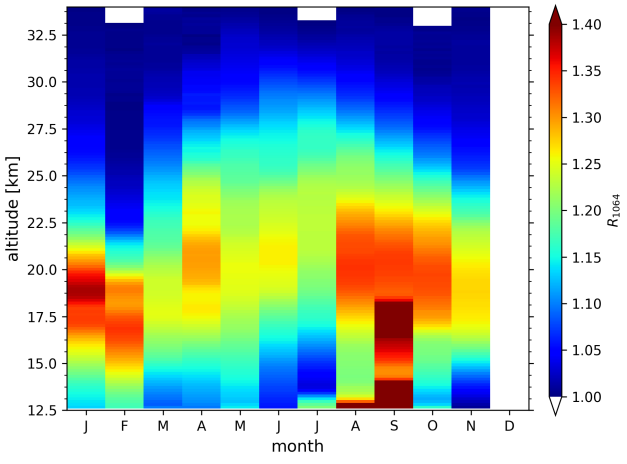

Figure 10. Mean seasonal cycle of aerosol backscatter ratio R_{1064} over the time span 2014 to 2017. The backscatter ratio was calculated from hourly averaged lidar data and averaged per month afterwards. The seasonal cycle is calculated from 208 measurement runs with a total of 3646 hours.